






Article

Structural and Biological Comparative Studies on M(II)-Complexes (M = Co, Mn, Cu, Ni, Zn) of Hydrazone-*s*-Triazine Ligand Bearing Pyridyl Arm

Mezna Saleh Altowyan ¹, Ayman El-Faham ^{2,3}, MennaAllah Hassan ³, Assem Barakat ⁴, Matti Haukka ⁵, Morsy A. M. Abu-Youssef ³, Saied M. Soliman ^{3,*} and Amal Yousri ^{3,*}

- ¹ Department of Chemistry, College of Science, Princess Nourah bint Abdulrahman University, P.O. Box 84428, Riyadh 11671, Saudi Arabia; msaltowyan@pnu.edu.sa
- ² Department of Clinical Sciences, College of Medicine, Dar Al Uloom University, P.O. Box 45142, Riyadh 11512, Saudi Arabia; ayman.a@dau.edu.sa or ayman.elfaham@alexu.edu.eg or aymanel_faham@hotmail.com
- ³ Department of Chemistry, Faculty of Science, Alexandria University, P.O. Box 426, Ibrahimia, Alexandria 21321, Egypt; menaallahhassanelsayed@gmail.com (M.H.); morsy5@alexu.edu.eg (M.A.M.A.-Y.)
- ⁴ Department of Chemistry, College of Science, King Saud University, P.O. Box 2455, Riyadh 11451, Saudi Arabia; ambarakat@ksu.edu.sa
- ⁵ Department of Chemistry, University of Jyväskylä, P.O. Box 35, FI-40014 Jyväskylä, Finland
- * Correspondence: saied1soliman@yahoo.com or saeed.soliman@alexu.edu.eg (S.M.S.); amal.yousri@alexu.edu.eg or amalyousri@yahoo.com (A.Y.)

Abstract: The molecular and supramolecular structures of some M(II) complexes (M = Co, Mn, Cu, Ni, Zn) with a hydrazone-*s*-triazine ligand (^{BM}PyTr) were discussed based on single crystal X-ray diffraction (SCXRD), Hirshfeld and DFT analyses. A new Co(II) complex of the same ligand was synthesized and its structure was confirmed to be [Co(^{BM}PyTr)Cl₂] \cdot H₂O based on FTIR and UV-Vis spectra, elemental analysis and SCXRD. The geometry around Co(II) was a distorted square pyramidal configuration ($\tau_5 = 0.4$), where Co(II) ion is coordinated to one NNN-tridentate ligand (^{BM}PyTr) and two Cl⁻ ions. A Hirshfeld analysis indicated all potential contacts within the crystal structure, where the percentages of O \cdots H, N \cdots H, C \cdots H, and H \cdots H contacts in one unit were 11.2, 9.3, 11.4, and 45.9%, respectively, while the respective values for the other complex unit were 10.3, 8.8, 10.6, and 48.0%. According to DFT calculations, the presence of strongly coordinating anions, such as Cl⁻, in addition to the large metal ion size, were found to be the main reasons for the small M-^{BM}PyTr interaction energies in the cases of [Mn(^{BM}PyTr)Cl₂] (260.79 kcal/mol) and [Co(^{BM}PyTr)Cl₂] \cdot H₂O (307.46 kcal/mol) complexes. Interestingly, the Co(II) complex had potential activity against both Gram-positive (*S. aureus* and *B. subtilis*) and Gram-negative (*E. coli* and *P. vulgaris*) bacterial strains with inhibition zone diameters of 13, 15, 16, and 18 mm, respectively. Also, the new [Co(^{BM}PyTr)Cl₂] \cdot H₂O (IC₅₀ = 131.2 \pm 6.8 μ M) complex had slightly better cytotoxic activity against HCT-116 cell line compared to ^{BM}PyTr (145.3 \pm 7.1 μ M).

Keywords: hydrazone-*s*-triazine; penta-coordinated Co(II) complex; Hirshfeld; DFT; cytotoxic activity; antimicrobial



Citation: Altowyan, M.S.; El-Faham, A.; Hassan, M.; Barakat, A.; Haukka, M.; Abu-Youssef, M.A.M.; Soliman, S.M.; Yousri, A. Structural and Biological Comparative Studies on M(II)-Complexes (M = Co, Mn, Cu, Ni, Zn) of Hydrazone-*s*-Triazine Ligand Bearing Pyridyl Arm. *Inorganics* **2024**, *12*, 268. <https://doi.org/10.3390/inorganics12100268>

Academic Editor: Graeme Hogarth

Received: 14 September 2024

Revised: 7 October 2024

Accepted: 11 October 2024

Published: 14 October 2024



Copyright: © 2024 by the authors. Licensee MDPI, Basel, Switzerland. This article is an open access article distributed under the terms and conditions of the Creative Commons Attribution (CC BY) license (<https://creativecommons.org/licenses/by/4.0/>).

1. Introduction

Heterocyclic rings play a crucial role as primary components in numerous compounds found in both natural and synthetic drugs [1,2]. Consequently, the scientific investigation of novel heterocyclic molecular systems has garnered significant attention from chemists due to their diverse applications [3–5]. Specifically, *s*-triazine heterocycles have shown interesting potential as energetic explosives and organic corrosion inhibitors [6]. Compounds containing both pyrazole and *s*-triazine rings have demonstrated minimal toxicity in terms of growth stimulation [7,8]. Furthermore, *s*-triazine derivatives displayed various anticancer activities, depending on the specific groups attached to the *s*-triazine core [8].

Additionally, *s*-triazines have a weak ligand field and can form stable high-spin metal complexes, leading to extended molecular and supramolecular architectures [9–11]. Moreover, *s*-triazine and its derivatives offer a diverse range of pharmacological benefits, including antibacterial, antiviral, anti-malarial, anti-inflammatory, anticancer, anti-leukemia, and anti-HIV activities, etc. [12–16]. Additionally, hydrazones with an azomethine -NHN=CH- group are a significant class of molecules that produce new compounds with a range of biological activities [17]. Also, they can be applied in dyes, nanoparticles, corrosion inhibition, the analysis of metal ions, and water treatment [18]. Furthermore, morpholine ring is already known as an active moiety in medicinal chemistry, either licensed or under investigation due to its beneficial features in biological and metabolic processes [19].

On the other hand, cobalt is a physiologically relevant metal. It plays a crucial role in numerous biological processes and exhibits significant biochemical activity as an essential trace metal [20]. Cobalt exists in two prevalent oxidation states, which are Co(II) and Co(III). The properties of the ligands are pivotal in determining the ultimate oxidation state of cobalt in its complexes. Recently, there has been a surge in the synthesis of cobalt complexes using multifunctional ligands [21–24]. Throughout the centuries, many cobalt complexes have been synthesized using multifunctional ligands, and they have been employed to inhibit the growth of harmful microorganisms [21–26]. This has led to the exploration and development of many new cobalt complexes, holding promise in the design and production of antibacterial agents to combat antibiotic-resistant microorganisms [27–29]. Cobalt complexes find extensive applications across diverse fields of human interest, encompassing antibacterial, antiviral, antifungal, antioxidant, anti-inflammatory, antischaemic, antiparasitic, antithrombotic, and antitumor agents [27–38]. This broad range of applications is attributed to the biological significance of cobalt and its synergistic activity with other drugs. Moreover, *s*-triazine ligands, in combination with cobalt, have been investigated for their potential as catalysts in chemical synthesis transformations and medical applications [2,39–47].

As a continuation of the interesting structural and the promising biological properties of *s*-triazine derivatives and their metal complexes, we presented here the synthesis and characterization of a new heteroleptic cobalt(II) complex with 2,4-*bis*(morpholin-4-yl)-6-[(*E*)-2-[1-(pyridin-2-yl)ethylidene]hydrazin-1-yl]-1,3,5-triazine as the ligand (^{BM}PyTr; Figure 1). Several characterization tools were utilized to study and confirm its structure, such as FTIR and UV–Vis spectroscopic techniques, as well as elemental analysis and single crystal X-ray diffraction (SCXRD). A comparative study for the molecular and supramolecular structure aspects, as well as the biological activity (antibacterial and anticancer) of the new complex with the structurally related complexes [48–50], is also presented. Theoretical DFT studies on the M-^{BM}PyTr affinity were performed to show the different factors which affect the interaction energy between the ligand ^{BM}PyTr and different metal ions.

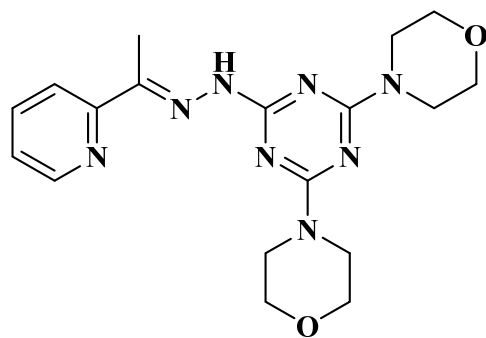
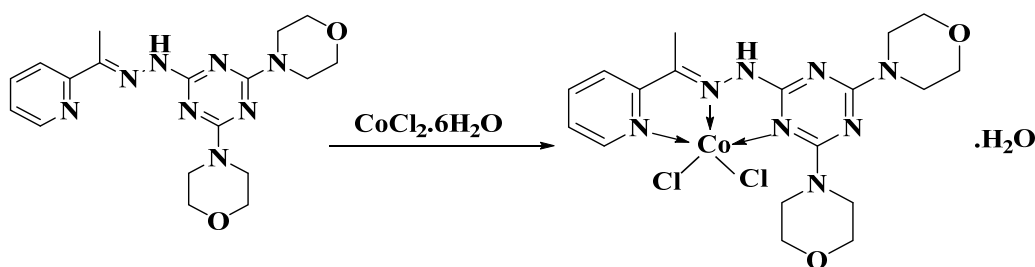


Figure 1. Structure of ^{BM}PyTr.

2. Results and Discussion

2.1. Synthesis and Characterization

The reaction of **BM**PyTr and $\text{CoCl}_2 \cdot 6\text{H}_2\text{O}$ in ethanol afforded a new heteroleptic complex $[\text{Co}(\text{BM}\text{PyTr})\text{Cl}_2] \cdot \text{H}_2\text{O}$ (Scheme 1). The structure of the complex was confirmed using elemental analysis, FTIR spectroscopy, and single crystal X-ray diffraction (SCXRD). The FTIR spectrum of the Co(II) complex showed distinct spectral bands at 1600 and 1569 cm^{-1} due to the $\nu_{(\text{C}=\text{N})}$ vibrations (Figure S1). The $\nu_{(\text{C}=\text{N})}$ mode is observed in the free ligand at 1584 cm^{-1} (Figure S2). The significant shifts in the $\nu_{(\text{C}=\text{N})}$ mode is a consequence of the complexation between Co(II) and **BM**PyTr via the triazine, azomethine, and pyridine nitrogen atoms. The $\nu_{(\text{C}=\text{C})}$ vibration was detected at 1500 and 1492 cm^{-1} in the FTIR spectrum of $[\text{Co}(\text{BM}\text{PyTr})\text{Cl}_2] \cdot \text{H}_2\text{O}$ and **BM**PyTr, respectively, showing little variation compared to the $\nu_{(\text{C}=\text{N})}$ mode.



Scheme 1. Synthesis of $[\text{Co}(\text{BM}\text{PyTr})\text{Cl}_2] \cdot \text{H}_2\text{O}$.

The UV–Vis spectra of the Co(II) complex and its free ligand **BM**PyTr ($2.5 \times 10^{-4} \text{ M}$) were measured in DMSO and ethanol as solvents (Figure 2). The spectral band observed in ethanol at 305 nm for **BM**PyTr could be assigned to the $n \rightarrow \pi^*$ transition. This band undergoes a bathochromic shift to 325 nm in the case of the Co(II) complex. The corresponding bands in DMSO are detected at 305 and 312 nm, respectively. In addition, the spectral bands observed at 230 and 235 nm for **BM**PyTr and $[\text{Co}(\text{BM}\text{PyTr})\text{Cl}_2] \cdot \text{H}_2\text{O}$ in ethanol could be assigned to the $\pi \rightarrow \pi^*$ transition. A new broad band appeared in the Co(II) complex at 415 and 405 nm in DMSO and ethanol, respectively. This band could be assigned to the d-d transition of the high-spin Co(II) complex [51].

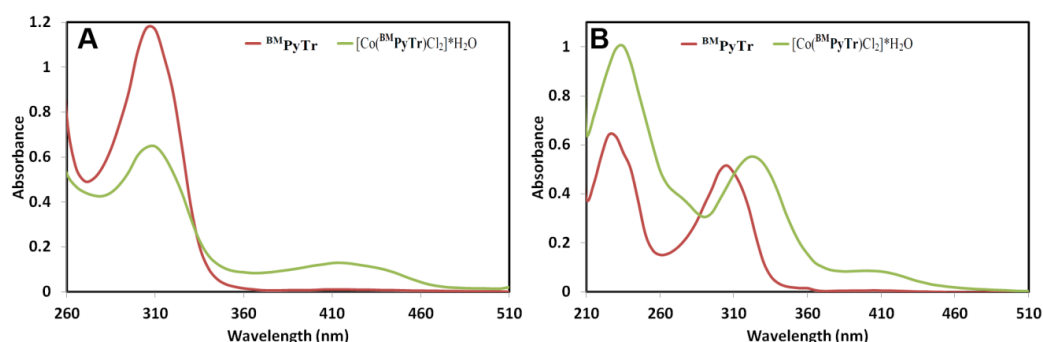


Figure 2. The UV–Vis spectra of $[\text{Co}(\text{BM}\text{PyTr})\text{Cl}_2] \cdot \text{H}_2\text{O}$ and **BM**PyTr in DMSO (A) and ethanol (B).

2.2. X-ray Structure Description

The structure of the studied complex was confirmed using X-ray crystallography to be $[\text{Co}(\text{BM}\text{PyTr})\text{Cl}_2] \cdot \text{H}_2\text{O}$ (**1**; Figure 3). It crystallized in the triclinic crystal system and $P-1$ space group. The unit cell parameters were $a = 8.50463(10)$, $b = 11.85531(14)$, $c = 22.1524(2) \text{ \AA}$, $\alpha = 84.2782(9)^\circ$, $\beta = 87.3524(9)^\circ$, and $\gamma = 89.2680(10)^\circ$. The number of molecules in the unit cell was four, while the unit cell volume and crystal density were $2219.94(4) \text{ \AA}^3$ and 1.593 mg/m^3 , respectively (Table 1).

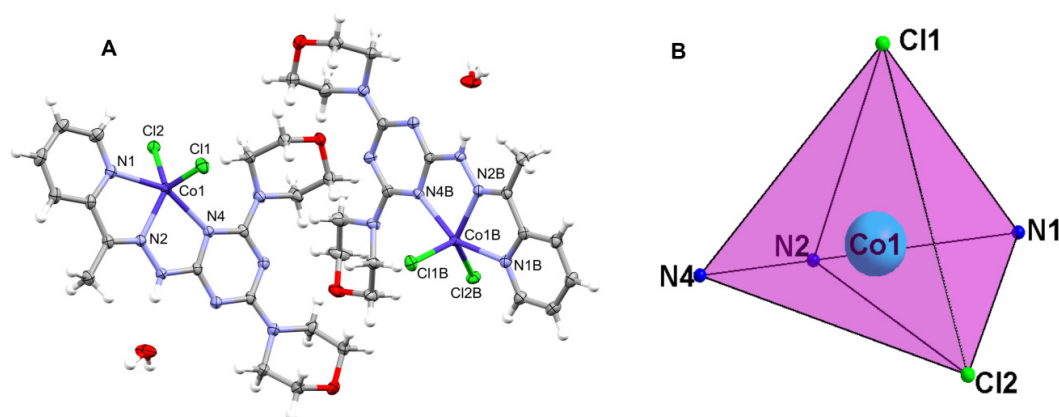


Figure 3. X-ray structure showing the numbering of the atom (A) and the distorted coordination geometry around Co1 (B) for $[\text{Co}(\text{BM PyTr})\text{Cl}_2]\cdot\text{H}_2\text{O}$.

Table 1. Crystal data for $[\text{Co}(\text{BM PyTr})\text{Cl}_2]\cdot\text{H}_2\text{O}$.

	$[\text{Co}(\text{BM PyTr})\text{Cl}_2]\cdot\text{H}_2\text{O}$
CCDC	2,340,998
empirical formula	$\text{C}_{18}\text{H}_{26}\text{Cl}_2\text{CoN}_8\text{O}_3$
fw	532.30
temp (K)	120(2)
λ (Å)	1.54184
cryst syst	Triclinic
space group	$P\bar{1}$
a (Å)	8.50463(10)
b (Å)	11.85531(14)
c (Å)	22.1524(2)
α (deg)	84.2782(9)
β (deg)	87.3524(9)
γ (deg)	89.2680(10)
V (Å ³)	2219.94(4)
Z	4
ρ_{calc} (Mg/m ³)	1.593
μ (Mo K α) (mm ⁻¹)	8.615
No. reflns.	89,427
Unique reflns.	9559
Completeness to $\theta = 67.684^\circ$	100%
GOOF (F^2)	1.093
R_{int}	0.0304
R_1^a ($I \geq 2\sigma$)	0.0270
wR_2^b ($I \geq 2\sigma$)	0.0724

$$^a R_1 = \sum ||F_o| - |F_c|| / \sum |F_o|, \quad ^b wR_2 = \{\sum [w(F_o^2 - F_c^2)^2] / \sum [w(F_o^2)^2]\}^{1/2}.$$

The structure of this complex showed two $[\text{Co}(\text{BM PyTr})\text{Cl}_2]\cdot\text{H}_2\text{O}$ molecules as an asymmetric formula, which were slightly different in their geometric parameters (Table 2). In this neutral complex, the Co(II) was penta-coordinated with two chloride ions and three nitrogen atoms from the **BM PyTr** ligand. There were three different Co-N interactions where the Co-N_(hydrazone) bonds were the shortest. The respective Co1-N2 and Co1B-N2B distances were determined to be 2.0360(13) and 2.0301(12) Å, respectively. The longest Co-N interactions were related to the Co-N_(s-triazine) where the corresponding Co1-N4 and Co1B-N4B distances were 2.1762(13) and 2.1919(12) Å, respectively. Hence, the order of the Co-N distances was Co-N_(hydrazone) < Co-N_(pyridine) < Co-N_(s-triazine). In the structurally related $[\text{Mn}(\text{BM PyTr})\text{Cl}_2]$ (2) and $[\text{Cu}(\text{BM PyTr})\text{Cl}_2]\cdot\text{H}_2\text{O}$ (3) complexes, the order of the metal to nitrogen distances was the same [51]. For example, the Mn-N_(hydrazone), Mn-

$N_{(\text{pyridine})}$, and $Mn-N_{(s\text{-triazine})}$ distances were 2.183(1), 2.264(2), and 2.428(1) Å, respectively. The bite angles of ${}^{\text{BM}}\text{PyTr}$ in **1** were 75.55(5)° (N2-Co1-N1) and 77.91(5)° (N2-Co1-N4) for one unit, and 75.82(5)° (N2B-Co1B-N1B) and 77.71(5)° (N2B-Co1B-N4B) for the other unit. In addition, there were two Co-Cl coordination interactions. In one unit, the Co1-Cl2 and Co1-Cl1 distances were 2.2909(4) and 2.3414(4) Å, respectively, while for the other unit, the Co1B-Cl2B and Co1B-Cl1B distances were 2.2840(4) and 2.3221(4) Å, respectively. The Cl-Co-Cl angles were 120.068(17) (Cl2-Co1-Cl1) and 122.675(17)° (Cl2B-Co1B-Cl1B). Therefore, the structure of the CoN_3Cl_2 coordination sphere could be described as a highly distorted penta-coordinated system. The Addison τ_5 parameter was calculated to be 0.35 for one unit and 0.37 for the other unit, with letter B in atom numbering. As a result, the structure could be described as a highly distorted penta-coordinated system which is close to square pyramidal [52]. These results for $[\text{Co}({}^{\text{BM}}\text{PyTr})\text{Cl}_2]\cdot\text{H}_2\text{O}$ (**1**) are found to be in good agreement with those for the $[\text{Mn}({}^{\text{BM}}\text{PyTr})\text{Cl}_2]$ (**2**) and $[\text{Cu}({}^{\text{BM}}\text{PyTr})\text{Cl}_2]\cdot\text{H}_2\text{O}$ (**3**) complexes, where the τ_5 values were calculated to be 0.33 and 0.24, respectively [48]. Hence, the square pyramidal configuration showed the lowest distortion in case of **3**. It is worth noting that the X-ray structure of **1** indicated the presence of one hydration water molecule in the outer sphere, which did not participate in the coordination with Co(II) but significantly contributed in the supramolecular structure of complex **1**.

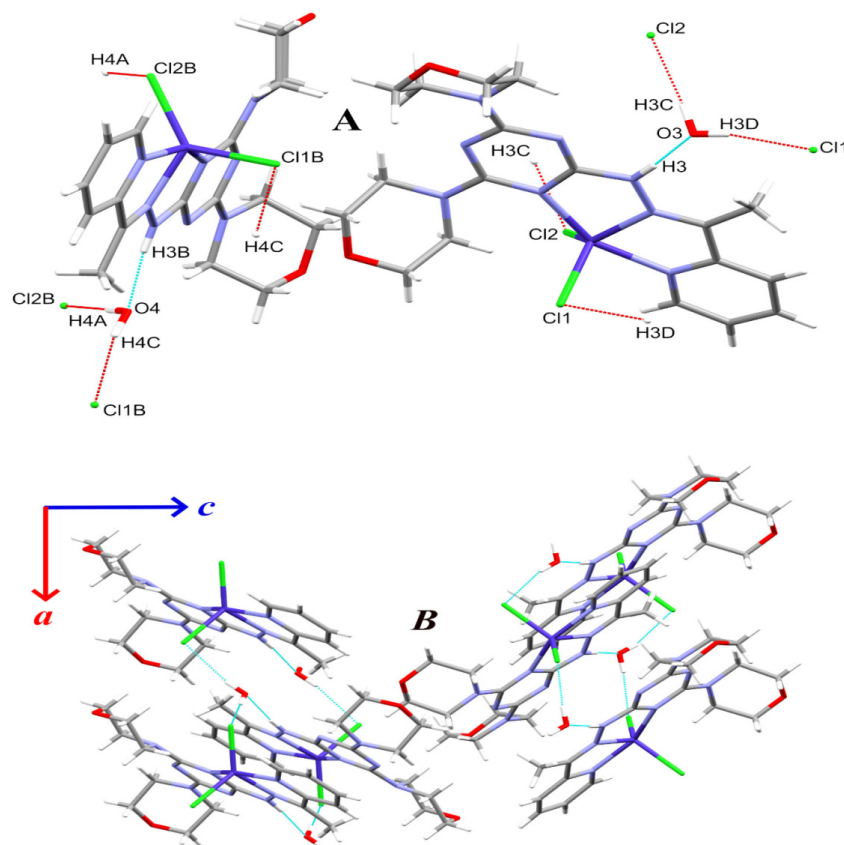
Table 2. Selected bond lengths (Å) and angles (°) for $[\text{Co}({}^{\text{BM}}\text{PyTr})\text{Cl}_2]\cdot\text{H}_2\text{O}$.

Bond Distances			
Co(1)-N(2)	2.0360(13)	Co(1B)-N(2B)	2.0301(12)
Co(1)-N(1)	2.1375(13)	Co(1B)-N(1B)	2.1459(13)
Co(1)-N(4)	2.1762(13)	Co(1B)-N(4B)	2.1919(12)
Co(1)-Cl(2)	2.2909(4)	Co(1B)-Cl(2B)	2.2840(4)
Co(1)-Cl(1)	2.3414(4)	Co(1B)-Cl(1B)	2.3221(4)
Bond angles			
N(2)-Co(1)-N(1)	75.55(5)	N(2B)-Co(1B)-N(1B)	75.82(5)
N(2)-Co(1)-N(4)	77.91(5)	N(2B)-Co(1B)-N(4B)	77.71(5)
N(1)-Co(1)-N(4)	153.21(5)	N(1B)-Co(1B)-N(4B)	152.95(5)
N(2)-Co(1)-Cl(2)	131.14(4)	N(2B)-Co(1B)-Cl(2B)	131.95(4)
N(1)-Co(1)-Cl(2)	90.03(4)	N(1B)-Co(1B)-Cl(2B)	90.80(4)
N(4)-Co(1)-Cl(2)	104.93(4)	N(4B)-Co(1B)-Cl(2B)	102.87(3)
N(2)-Co(1)-Cl(1)	107.06(4)	N(2B)-Co(1B)-Cl(1B)	104.10(4)
N(1)-Co(1)-Cl(1)	91.95(4)	N(1B)-Co(1B)-Cl(1B)	92.45(4)
N(4)-Co(1)-Cl(1)	99.20(3)	N(4B)-Co(1B)-Cl(1B)	99.31(4)
Cl(2)-Co(1)-Cl(1)	120.07(2)	Cl(2B)-Co(1B)-Cl(1B)	122.68(2)

The supramolecular structure of **1** is controlled by two types of non-covalent interactions, which are the N-H...O and O-H...Cl hydrogen bonds (Table 3). The presentation of these hydrogen bond contacts is shown in Figure 4A. There are two significant N-H...O hydrogen bonds, which occurred between the N-H of the hydrazone linkage as a hydrogen-bond donor and the freely un-coordinated O-atom from the crystal water molecule as hydrogen-bond acceptor. The hydrogen to acceptor distances were 1.92(2) and 2.00(2) Å for N3-H3...O3 and N3B-H3B...O4, respectively, while the donor to acceptor distances were 2.7737(19) and 2.8074(18) Å, respectively. Furthermore, there were four O-H...Cl interactions, which occurred between the crystal water hydrogen atoms as hydrogen-bond donor and the coordinated chloride anion as hydrogen-bond acceptor. In this case, the hydrogen to acceptor (Cl) distances ranged from 2.29(3) Å (O3-H3C...Cl2) to 2.45(3) Å (O4-H4C...Cl1B), while the donor (O) to acceptor (Cl) distances ranged from 3.1605(15) to 3.2639(14) Å, respectively. The resulting hydrogen packing scheme is shown in Figure 4B. Hence, the supramolecular structure of complex **1** could be described as a hydrogen bonding network extended along the *a*-direction.

Table 3. Hydrogen bonds for [Co(^{BM}PyTr)Cl₂]·H₂O (Å and °).

D-H···A	d(D-H)	d(H···A)	d(D···A)	<(DHA)	Symmetry Codes
N(3)-H(3)···O(3)	0.85(2)	1.92(2)	2.7737(19)	175(2)	
N(3B)-H(3B)···O(4)	0.81(2)	2.00(2)	2.8074(18)	173(2)	
O(3)-H(3D)···Cl(1)	0.83(3)	2.43(3)	3.2414(15)	167(3)	-x - 1, -y + 1, -z + 2
O(3)-H(3C)···Cl(2)	0.88(3)	2.29(3)	3.1605(15)	176(3)	-x, -y + 1, -z + 2
O(4)-H(4C)···Cl(1B)	0.83(3)	2.45(3)	3.2639(14)	169(3)	-x, -y + 1, -z + 1
O(4)-H(4A)···Cl(2B)	0.87(3)	2.31(3)	3.1865(14)	177(3)	-x + 1, -y + 1, -z + 1

**Figure 4.** The important H-bond contacts (A) and the corresponding packing scheme (B) for [Co(^{BM}PyTr)Cl₂]·H₂O.

Interestingly, the X-ray structure analysis indicated the presence of some anion- π interactions occurred between the coordinated chloride anion and the pyridine π -system. There were three Cl···C_(pyridine) interactions which were different in their distances (Table 4). In one unit, the Cl2···C1_(pyridine) distance was 3.420(2) Å, while for the other unit, the Cl2B···C1B_(pyridine) and Cl2B···C2B_(pyridine) distances were 3.444(2) and 3.437(2) Å, respectively (Figure 5). In complex **3**, there was one short Cl···C contact (3.427(2) Å) which was detected, while no anion- π interactions were observed in case of **2**.

Table 4. Anion- π stacking contacts for **1**.

Contact	Length (Å)	Symm. Code
Cl(2)···C(1)	3.420(2)	-x, -y, 2 - z
Cl(2B)···C(1B)	3.444(2)	1 - x, 2 - y, 1 - z
Cl(2B)···C(2B)	3.437(2)	1 - x, 2 - y, 1 - z

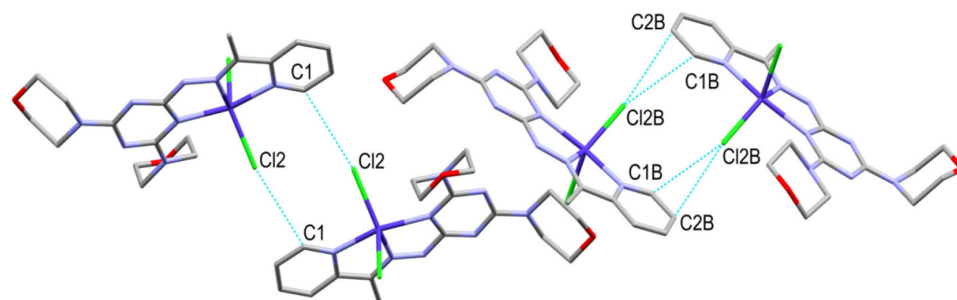


Figure 5. The anion- π stacking interactions that occurred in **1**.

2.3. Hirshfeld Analysis

The stability of the crystal structure results from various forces that maintain the molecules in a specific arrangement. Hirshfeld calculations could provide a complete picture about the forces which are responsible for the supramolecular structure of organic and inorganic compounds [53–61]. The d_{norm} maps for complex **1** are shown in Figure 6. The curvedness and shape index surfaces are shown in Figure S3.

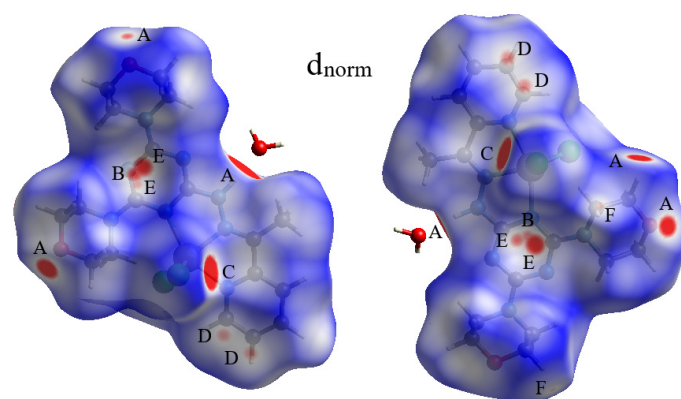


Figure 6. Full d_{norm} map for $[\text{Co}(\text{BMpyTr})\text{Cl}_2]\cdot\text{H}_2\text{O}$. The most important interactions are (A) $\text{O}\cdots\text{H}$, (B) $\text{N}\cdots\text{H}$, (C) $\text{Cl}\cdots\text{H}$, (D) $\text{C}\cdots\text{C}$, (E) $\text{C}\cdots\text{H}$, and (F) $\text{H}\cdots\text{H}$.

With the aid of Hirshfeld calculations, all potential contacts within the crystal structure are collected in Table S1. The results of the quantitative analysis for the different intermolecular interactions in complex **1** are shown in Figure 7. For one unit, the percentages of $\text{Cl}\cdots\text{H}$, $\text{O}\cdots\text{H}$, $\text{N}\cdots\text{H}$, $\text{C}\cdots\text{H}$, and $\text{H}\cdots\text{H}$ are 16.7, 11.2, 9.3, 11.4, and 45.9%, respectively. The respective values for the unit with letter B in the atom numbering are 16.8, 10.3, 8.8, 10.6, and 48.0%, respectively. In case of complex **2**, their percentages are 20.9, 8.9, 8.1, 7.1, and 45.8%, respectively [48].

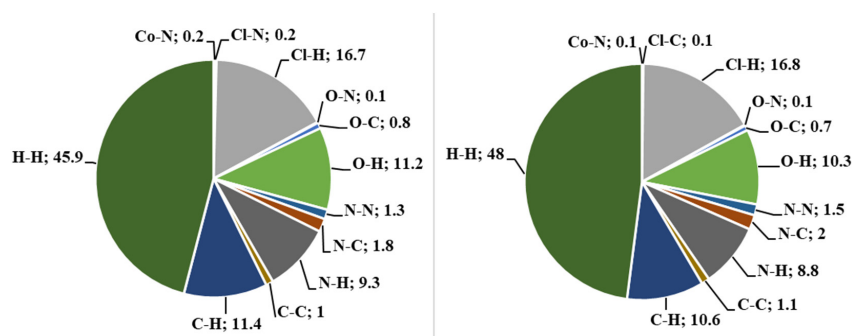


Figure 7. The percentages of close contacts in the two units of **1**.

The fingerprint plots shown in Figure 8 and Figure S4 revealed many strong intermolecular contacts. The d_{norm} map provides a summary of all short contacts, represented by red and white areas, signifying interaction distances shorter or equal to the van der Waals radii sum of the interacting atoms, respectively. Conversely, contacts longer than the van der Waals radii sum of the interacting atoms appear as blue-colored regions. The d_{norm} map indicated the importance of Cl···H, O···H, N···H, C···C, C···H, and H···H interactions in the molecular packing of **1**. The shortest Cl···H, O···H, N···H, and C···H contacts are Cl2···H3C (2.180 Å), O3···H3 (1.768 Å), N7···H16C (2.534 Å), and C9···H16C (2.608 Å), respectively. For C···C interactions, the C1···C2 (3.329 Å) and C1B···C2B (3.319 Å) are the shortest (Table S1). In addition, there are short H···H interactions which are the H3A···H13C (2.147 Å) and H14A···H18C (2.154 Å). In **2**, the shortest Cl···H (2.532 Å) and O···H (2.477 Å) contacts are generally longer than those detected in **1** [48].

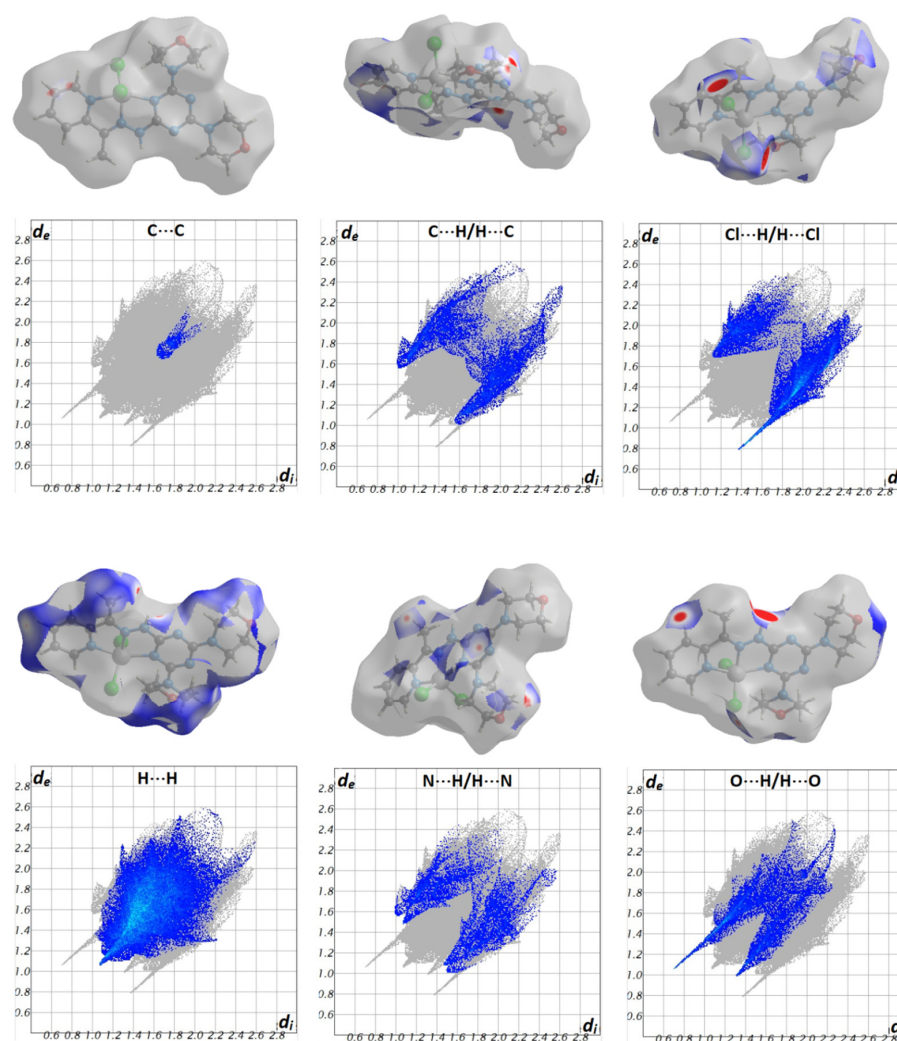


Figure 8. The decomposed d_{norm} maps and fingerprint plots for significant contacts in **1**.

2.4. Enrichment Ratio

The possibility of each atom pair in the crystal to make intermolecular interaction was investigated by calculating the enrichment ratio (E_{XY}) [62]. The results of the enrichment ratio are depicted in Table 5. Since the enrichment ratios for the Cl···H, O···H, N···C, and H···C are greater than the unity, each of these atom pairs have a high probability for carrying out intermolecular interactions in the crystal structure. The rest of the other contacts with an enrichment ratio less than the unity have a low possibility of occurring.

Table 5. Enrichment ratio calculations for 1.

Contact	%C ^a	%R ^b	E _{XY}	Atom	%S ^c
Cl···H	16.7	11.9	1.4	H	70.2
O···C	0.8	1.0	0.8	O	6.05
O···H	11.2	8.5	1.3	N	7.1
N···C	1.8	1.1	1.6	C	8
N···H	9.3	10.0	0.9	Cl	8.45
H···C	11.4	11.2	1.0		
H···H	45.9	49.3	0.9		
Cl···N	0.2	1.2	0.2		

^a %contact ^b ratio of random contact ^c %contribution for a chemical species X.

2.5. Energy Framework Analysis

The energy framework is crucial for comprehending the various energy types that play a role in the supramolecular assembly of molecules within crystals [63–74]. Table S2 provides an energy breakdown, including the contributions of different components (E_{ele} , E_{pol} , E_{dis} , E_{rep} , and E_{tot}). The results provide the total interaction energy (E_{tot}) of -594.4 kJ/mol involving the electrostatic (-233.351 kJ/mol), polarization (-152.334 kJ/mol), dispersion (-427.525 kJ/mol), and repulsion (218.646 kJ/mol). It is obvious that, the Cl···H interaction between the central molecule and the $-x$, $-y$, $-z$ symmetry water molecules (turquoise and magenta) are the strongest among near neighbors, with a total energy of -125.2 kJ/mol for each (Figure S5). The total energy diagram showed a strong resemblance to the dispersion energy frameworks (Figure 9), suggesting their significant contribution to the total forces in crystal packing.

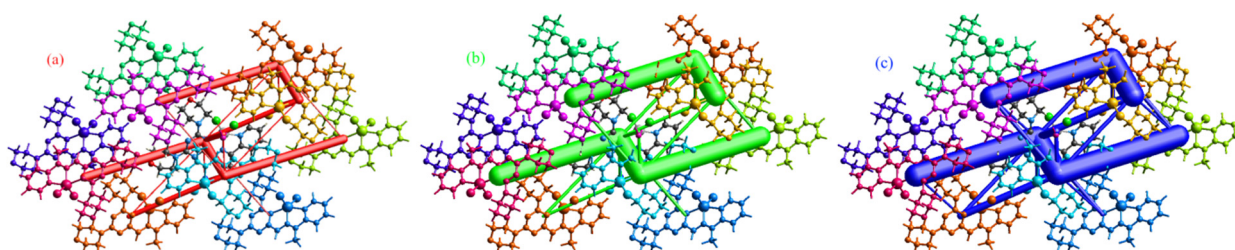


Figure 9. Energy framework diagram for separate electrostatic (a), dispersion (b), and total interaction energy (c). The cylinder thicknesses indicated the relative strengths of interactions between molecules.

2.6. Comparative DFT Study

Density functional theory (DFT) calculations were conducted utilizing the X-ray structure coordinates for energy computations of the $[M\text{-}^{\text{BM}}\text{PyTr}]^{2+}$ systems. A comparative analysis of the ligand's affinity towards various divalent metal ions was performed for complexes 1–3, $[\text{Zn}(\text{BM}\text{PyTr})(\text{NO}_3)_2]$; 4, $[\text{Zn}(\text{BM}\text{PyTr})(\text{NCS})_2]$; 5 $[\text{Cu}(\text{BM}\text{PyTr})(\text{NO}_3)_2]$; 6, $[\text{Ni}(\text{BM}\text{PyTr})(\text{H}_2\text{O})_3](\text{NO}_3)_2 \cdot 3\text{H}_2\text{O}$; 7, and $[\text{Ni}(\text{BM}\text{PyTr})(\text{H}_2\text{O})_3](\text{NO}_3)_2 \cdot \text{H}_2\text{O}$; 8 [48–50]. Then, the computed energies were used to calculate the M-^{BM}PyTr interaction energies as described in Table 6. The Co(II)-^{BM}PyTr interaction energy (E_{int}) was computed to be 307.46 kcal/mol (average value). On the other hand, the M-^{BM}PyTr interaction energies were calculated to be 260.79, 366.09, -322.23 , -314.89 , 364.27, -356.37 , and 361.57 kcal/mol for complexes 2–8, respectively. Since, all the studied systems comprised a divalent metal ion, there are two main factors affecting the M-^{BM}PyTr interaction energies, which are the metal ion size and the nature of other coordinating ligand. The small-size metal ion has higher positive charge density, leading to higher interaction energy with ^{BM}PyTr. In contrast, strongly coordinating anions such as Cl^- significantly reduce the positive charge density of the metal ion compared to either the weakly coordinating anion such as NO_3^- and SCN^- or a neutral ligand such as H_2O . In this regard, the least M-^{BM}PyTr interaction

energy was detected in case of complexes **1** and **2**. The order of the M-^{BM}PyTr interaction energy is predicted to be **2** < **1** < **5** < **4** < **7** < **8** < **6** < **3**.

Table 6. The calculated M(II)–^{BM}PyTr interaction energies using ωB97XD method.

No.	Complex	M(II)	^{BM} PyTr	M(II)+ ^{BM} PyTr	[M(II)– ^{BM} PyTr] ²⁺	E _{int} ^a (kcal/mol)
1A	[Co(^{BM} PyTr)Cl ₂].H ₂ O	–1381.84	–1288.52	–2670.36	–2670.85	–311.54
1B	[Co(^{BM} PyTr)Cl ₂].H ₂ O ^b	–1381.84	–1288.54	–2670.38	–2670.86	–303.38
2	[Mn(^{BM} PyTr)Cl ₂]	–1150.15	–1288.57	–2438.72	–2439.13	–260.79
3	[Cu(^{BM} PyTr)Cl ₂].H ₂ O	–1639.50	–1288.56	–2928.06	–2928.64	–366.09
4	[Zn(^{BM} PyTr)(NO ₃) ₂]	–1778.45	–1288.49	–3066.95	–3067.47	–322.23
5	[Zn(^{BM} PyTr)(NCS) ₂]	–1778.45	–1288.48	–3066.94	–3067.44	–314.89
6	[Cu(^{BM} PyTr)(NO ₃) ₂]	–1639.50	–1364.96	–3004.46	–3005.04	–364.27
7	[Ni(^{BM} PyTr)(H ₂ O) ₃](NO ₃) ₂ .3H ₂ O	–1507.30	–1288.55	–2795.85	–2796.42	–356.37
8	[Ni(^{BM} PyTr)(H ₂ O) ₃](NO ₃) ₂ .H ₂ O	–1507.30	–1288.55	–2795.85	–2796.42	–361.57

^a E_{int} = E_{complex} – (E_{metal} + E_{ligand}) and ^b unit with letter B in atom numbering.

2.7. Biological Studies

2.7.1. Antimicrobial Assay

The efficiency of [Co(^{BM}PyTr)Cl₂].H₂O as an antimicrobial agent against selected harmful microbes was tested and the results are compared with other reported metal complexes [48,50] (Table 7). Complex **1** showed no activity against the studied fungal species as no zones for inhibitions were detected in the cases of *A. fumigatus* and *C. albicans*. In contrast, this complex showed good activity against both Gram-positive and Gram-negative bacterial strains. Regarding the Gram-positive bacteria, *S. aureus* and *B. subtilis*, the inhibition zones were 13 and 15 mm, respectively, while for the Gram-negative bacteria, *E. coli* and *P. vulgaris*, the inhibition zones were 16 and 18 mm, respectively. The initial assessment of the antimicrobial activity indicated the better action of the [Co(^{BM}PyTr)Cl₂].H₂O complex against the Gram-negative bacteria compared to the Gram-positive bacteria.

Table 7. Antimicrobial activities of ^{BM}PyTr and its complexes ^a.

Microorganism	^{BM} PyTr	1	2 ^f	3 ^f	4 ^g	5 ^g	Control
<i>S. aureus</i>	NA ^b (ND) ^c	13(1250)	11(2500)	18(625)	14(625)	15(625)	24(78) ^d
<i>B. subtilis</i>	NA ^b (ND) ^c	15(625)	19(312)	20(312)	15(625)	16(312)	26(39) ^d
<i>E. coli</i>	NA ^b (ND) ^c	16(156)	10(2500)	NA(ND)	NA ^b (ND) ^c	NA ^b (ND) ^c	30(10) ^d
<i>P. vulgaris</i>	NA ^b (ND) ^c	18(78)	12(1250)	14(1250)	18(156)	20(78)	25(5) ^d
<i>A. fumigatus</i>	NA ^b (ND) ^c	-	NA ^b (ND) ^c	NA ^b (ND) ^c	10(625)	NA ^b (ND) ^c	17(5) ^e
<i>C. albicans</i>	NA ^b (ND) ^c	-	8(5000)	NA ^b (ND) ^c	9(625)	10(312)	20(5) ^e

^a Inhibition zone diameter; mm (MIC; μg/mL) ^b NA: No activity; ^c ND: Not determined; ^d Gentamicin; ^e Ketoconazole; ^f [48]; and ^g [50].

On the other hand, the minimum inhibitory concentrations (MICs) for the [Co(^{BM}PyTr)Cl₂].H₂O complex against the studied bacteria are given in Table 7. The MIC values for this complex against *S. aureus* and *B. subtilis* were 1250 and 625 μg/mL, respectively. For *E. coli* and *P. vulgaris*, the MIC values were 156 and 78 μg/mL, respectively. Accordingly, the [Co(^{BM}PyTr)Cl₂].H₂O complex showed better activity against *P. vulgaris*, while it showed moderate activity compared with gentamicin as a positive control. It is worth noting that the free ligand showed no antibacterial activity under the same experimental conditions. Also, the results of the antimicrobial activities of the studied complex were compared with the structurally related [Mn(^{BM}PyTr)Cl₂]; **2**, [Cu(^{BM}PyTr)Cl₂].H₂O; **3**, [Zn(^{BM}PyTr)(NO₃)₂]; **4**, and [Zn(^{BM}PyTr)(NCS)₂]; **5** complexes. In this regard, the new Co(II) complex showed better activity against *S. aureus*, *E. coli*, and *P. vulgaris* compared to the [Mn(^{BM}PyTr)Cl₂] complex. The latter has inhibition zones of 11, 10, and 12 mm, respectively, while the MIC values were 2500, 2500, and 1250 μg/mL, respectively. Also, **1** showed better activity against the Gram-negative bacteria (*E. coli*) compared to the

[Cu(^{BM}PyTr)Cl₂]·H₂O, [Zn(^{BM}PyTr)(NO₃)₂], and [Zn(^{BM}PyTr)(NCS)₂] analogs (Table 7). Furthermore, **1** had better activity towards the Gram-negative bacteria (*P. vulgaris*) in comparison to the [Cu(^{BM}PyTr)Cl₂]·H₂O complex.

2.7.2. Cytotoxicity Assessments

The in vitro cytotoxic activities of the free ligand and the [Co(^{BM}PyTr)Cl₂]·H₂O complex against human colon HCT-116 and lung A-549 cancer cell lines using MTT assay were determined and compared with the structurally related [Mn(^{BM}PyTr)Cl₂], [Cu(^{BM}PyTr)Cl₂]·H₂O, [Zn(^{BM}PyTr)(NO₃)₂], and [Zn(^{BM}PyTr)(NCS)₂] complexes [48,50]. The %viability is drawn against the concentration in μM in order to determine the IC₅₀ of the synthesized complexes (Figure 10). The results clearly revealed the good cytotoxicity of the ligand (^{BM}PyTr) and their metal complexes **1–5** against both cell lines.

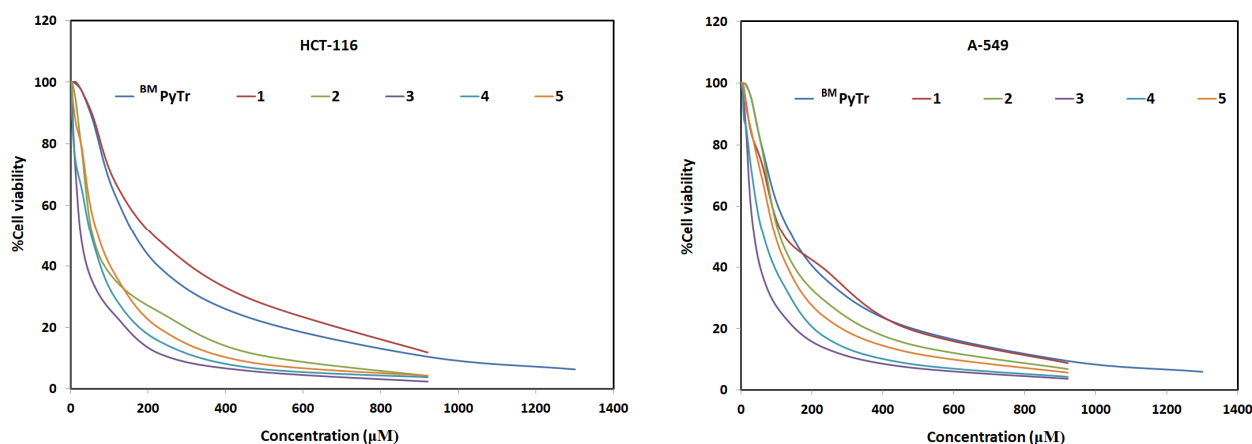
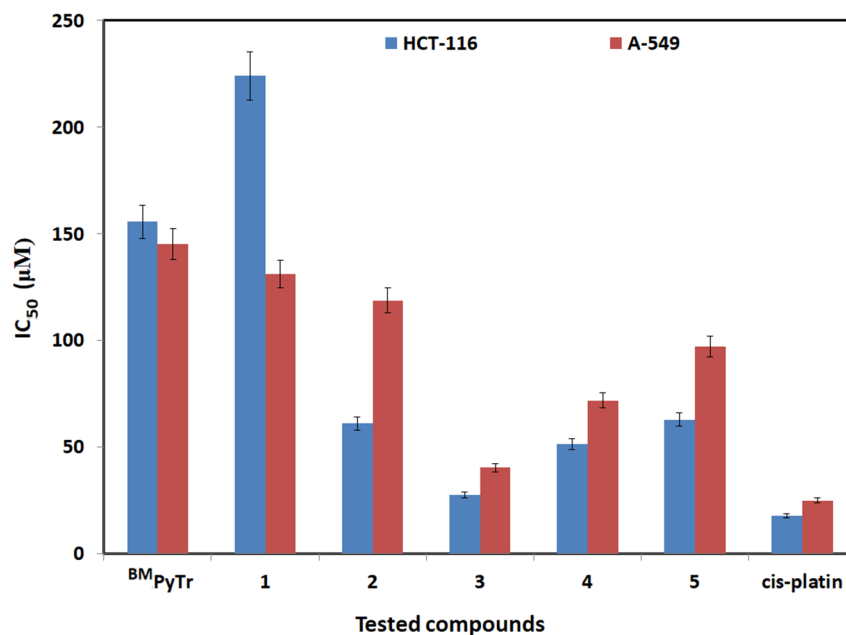


Figure 10. The viability assay for the free ligand (^{BM}PyTr), [Co(^{BM}PyTr)Cl₂]·H₂O (**1**), [Mn(^{BM}PyTr)Cl₂] (**2**), [Cu(^{BM}PyTr)Cl₂]·H₂O (**3**), [Zn(^{BM}PyTr)(NO₃)₂] (**4**), and [Zn(^{BM}PyTr)(NCS)₂] (**5**). All experiments were carried out in triplicate and the detailed results of the cell viability are given in Tables S4–S15.

In addition, the IC₅₀ values of the free ligand and its metal(II) complexes are compared with the standard drug *cis*-platin as a reference drug (Table 8 and Figure 11). The free ligand has the highest IC₅₀ value of 145.3 ± 7.1 μM against the colon carcinoma HCT-116 cell line, while for the complexes **1–5**, the IC₅₀ values are 131.2 ± 6.8, 118.8 ± 6.0, 40.3 ± 2.3, 51.46 ± 2.16, and 62.81 ± 2.82 μM. On the other hand, the IC₅₀ values for these complexes against lung carcinoma A-549 cell line are 224.0 ± 10.3, 61.0 ± 2.5, 27.7 ± 1.1, 71.88 ± 5.07, and 97.26 ± 5.07 μM, respectively, while the free ligand has an IC₅₀ value of 155.7 ± 7.6 μM. For *cis*-platin, the IC₅₀ values are 17.8 ± 1.6 and 24.9 ± 1.7 μM, respectively. Hence, the Cu(II) complex showed the highest potency against both cell lines [48,50] compared to the Co(II), Zn(II) and Mn(II) complexes, while the [Co(^{BM}PyTr)Cl₂]·H₂O complex had the lowest efficiency as an anticancer agent against both cell lines. It is worth noting that the cytotoxicity activity of all complexes was improved (except complex **1** against the HCT-116 cell line) compared to the free ligand for both cell lines. Examining the cytotoxic effect of CoCl₂ against the A-549 cancer cell line indicated no activity for the metal salt [75] (Table S15). As a result, the enhanced cytotoxic effect of **1** could be attributed to the complex rather than the free ^{BM}PyTr or CoCl₂. Interestingly, complexes **1–3**, which had the same coordination sphere but differed in the metal ion, were found to have different activities, as shown in Table 8. In this regard, the variation in the metal ion had a significant impact on the cytotoxic effects of the studied complexes.

Table 8. The IC₅₀ (μM) for ^{BM}PyTr and complexes 1–5 against HCT-116 and A-549 cell lines.

Cell Line	HCT-116	A-549
^{BM} PyTr	155.7 ± 7.6	145.3 ± 7.1
1	224.0 ± 10.3	131.2 ± 6.8
2	61.0 ± 2.5	118.8 ± 6.0
3	27.7 ± 1.1	40.3 ± 2.3
4	51.46 ± 2.16	71.88 ± 5.07
5	62.81 ± 2.82	97.26 ± 5.07
cis-platin	17.8 ± 1.6	24.9 ± 1.7

**Figure 11.** The IC₅₀ (μM) for ^{BM}PyTr and complexes 1–5 against HCT-116 and A-549 cell lines.

3. Materials and Methods

3.1. Materials and Physical Characterizations

A description of the materials and instrumentation used in this work are summarized in the Supplementary Data.

3.2. Synthesis of ^{BM}PyTr

The ligand (^{BM}PyTr) was prepared according to the method mentioned by our research group [48,49] (Method S1).

3.3. Synthesis of [Co(^{BM}PyTr)Cl₂] \cdot H₂O

The metal complex was synthesized by mixing 10 mL ethanolic solution of CoCl₂ \cdot 6H₂O (47.6 mg, 0.2 mmol) with a 10 mL ethanolic solution of ^{BM}PyTr (77.0 mg, 0.2 mmol). This mixture was filtered and allowed to evaporate slowly at RT. After approximately three days, dark purple crystals formed, which were then collected by filtration.

[Co(^{BM}PyTr)Cl₂] \cdot H₂O; m.p > 350°C; Yield 89%; Anal. Calc. for C₁₈H₂₆Cl₂CoN₈O₃: C, 40.62; H, 4.92; N, 21.05; Co, 11.07%. Found: C, 40.39; H, 4.84; N, 20.91; Co, 10.98%. IR (KBr, cm⁻¹): 3403 ν (O-H)_{water}, 3222 ν (N-H), 2964, 2919, 2858 ν (C-H), 1600, 1569 ν (C=N), 1501 ν (C=C), 1258 ν (C-N), 1391 ν (N-O). The FTIR spectra of the complex and the free ligand are shown in Figures S1 and S2, respectively.

3.4. Crystal Structure Determination

The crystal structure of $[\text{Co}(\text{BMPyTr})\text{Cl}_2]\cdot\text{H}_2\text{O}$ was measured following the procedures described in Method S2 [76–79].

3.5. Hirshfeld Analysis

The Crystal Explorer Ver. 17 program was used to perform Hirshfeld analysis [80,81]. Details for the protocol used to perform the energy framework analysis are found in Method S3 [63–74].

3.6. Computational Details

The calculations were conducted using the X-ray structure coordinates, employing the ωB97XD method [82] with the aid of Gaussian 09 program [83,84]. The TZVP basis sets were employed for all atoms. The calculations were performed for the free M(II) and BMPyTr as well as their complex species $[\text{M}^{\text{BMPyTr}}]^{2+}$.

3.7. Biological Studies

The anticancer [85] and antimicrobial [86] activities were assessed using the protocols outlined in Methods S4 and S5.

4. Conclusions

The heteroleptic $[\text{Co}(\text{BMPyTr})\text{Cl}_2]\cdot\text{H}_2\text{O}$ complex was synthesized and its structure was confirmed with the aid of elemental analysis, FTIR, UV–Vis spectra, and X-ray crystallography. The Co(II) had a penta-coordination environment with a highly distorted square pyramidal configuration. Using Hirshfeld surface analysis, the most dominant interaction was that of the hydrogenic $\text{H}\cdots\text{H}$ contacts (45.9–48%). Additionally, the presence of short $\text{Cl}\cdots\text{C}$ contacts indicated the existence of anion– π stacking interactions. DFT calculations explored the effect of metal ion size and the nature of coordinating ligands on the M(II)- BMPyTr interaction energies, where the Mn(II)- BMPyTr and Co(II)- BMPyTr interaction energies were the lowest. The free ligand (BMPyTr) and its $[\text{Co}(\text{BMPyTr})\text{Cl}_2]\cdot\text{H}_2\text{O}$ complex were tested for their cytotoxicity against the HCT-116 and A-549 cancer cell lines using the MTT assay, and the results were compared with the structurally related complexes. All complexes showed improved activity (except **1** versus HCT-116 cells) compared to BMPyTr . The improvement of the activity confirmed the important role of metal ions on the biological activity of the studied metal- BMPyTr complexes. Despite the free ligand (BMPyTr) having no antimicrobial activity, its metal(II) complexes showed diverse activities against the studied microbes. The $[\text{Co}(\text{BMPyTr})\text{Cl}_2]\cdot\text{H}_2\text{O}$ complex demonstrated good activity against both Gram-positive (*S. aureus* and *B. subtilis*) and Gram-negative bacteria (*E. coli* and *P. vulgaris*).

Supplementary Materials: The following supporting information can be downloaded at: <https://www.mdpi.com/article/10.3390/inorganics12100268/s1>, Figure S1: The FTIR spectra of the $[\text{Co}(\text{BMPyTr})\text{Cl}_2]\cdot\text{H}_2\text{O}$; Figure S2: The FTIR spectra of the free ligand (BMPyTr); Figure S3: The curvedness and shape index surfaces for the $[\text{Co}(\text{BMPyTr})\text{Cl}_2]\cdot\text{H}_2\text{O}$ complex; Figure S4: The fingerprint plots for the unit with letter B in the atom numbering for $[\text{Co}(\text{BMPyTr})\text{Cl}_2]\cdot\text{H}_2\text{O}$ complex; Figure S5: Visualization of molecular interactions within a cluster with a radius of 3.8 Å between the central molecule under investigation and its neighboring molecules, viewed along the *a*-axis; Figure S6: ^1H NMR of the ligand in CDCl_3 ; Figure S7: ^{13}C NMR of the ligand in CDCl_3 ; Table S1: The short intermolecular interactions in the $[\text{Co}(\text{BMPyTr})\text{Cl}_2]\cdot\text{H}_2\text{O}$; Table S2: Different interaction energies of the molecular pairs in kJ/mol; Table S3: Evaluation of anticancer activity against HCT-116 cell line for BMPyTr ; Table S4: Evaluation of anticancer activity against HCT-116 cell line for **1**; Table S5: Evaluation of anticancer activity against HCT-116 cell line for **2**; Table S6: Evaluation of anticancer activity against HCT-116 cell line for **3**; Table S7: Evaluation of anticancer activity against HCT-116 cell line for **4**; Table S8: Evaluation of anticancer activity against HCT-116 cell line for **5**; Table S9: Evaluation of anticancer activity against A-549 cell line for BMPyTr ; Table S10: Evaluation of anticancer activity against A-549 cell line for **1**; Table S11: Evaluation of anticancer activity against A-549 cell line for **2**; Table S12: Evaluation of anticancer activity against A-549 cell line for **3**; Table S13:

Evaluation of anticancer activity against A-549 cell line for **4**; Table S14: Evaluation of anticancer activity against A-549 cell line for **5**; Table S15: Evaluation of anticancer activity against A-549 cell line for CoCl_2 ; Method S1: Synthesis of ligand (BM PyTr); Method S2: Crystal structure determination; Method S3: Energy framework analysis protocol; Method S4: Evaluation of anticancer activity; Method S5: Evaluation of antimicrobial activity.

Author Contributions: Conceptualization, M.A.M.A.-Y., A.Y., A.E.-F. and S.M.S.; methodology, M.H. (MennaAllah Hassan), M.S.A. and A.Y.; software, M.H. (Matti Haukka), A.Y. and S.M.S.; validation, A.E.-F., A.Y. and A.B.; formal analysis, M.H. (MennaAllah Hassan), M.H. (Matti Haukka) and A.Y.; investigation, All authors; resources, A.E.-F., A.B., M.S.A. and S.M.S.; data curation, M.H. (MennaAllah Hassan) and A.Y.; writing—original draft preparation, All authors; writing—review and editing, All authors; supervision, M.A.M.A.-Y., A.Y., A.E.-F. and S.M.S.; funding acquisition, M.S.A. All authors have read and agreed to the published version of the manuscript.

Funding: Princess Nourah bint Abdulrahman University Researchers Supporting Project number (PNURSP2024R86), Princess Nourah bint Abdulrahman University, Riyadh, Saudi Arabia.

Data Availability Statement: The original contributions presented in the study are included in the article/Supplementary Materials, further inquiries can be directed to the corresponding authors.

Acknowledgments: Princess Nourah bint Abdulrahman University Researchers Supporting Project number (PNURSP2024R86), Princess Nourah bint Abdulrahman University, Riyadh, Saudi Arabia.

Conflicts of Interest: The authors declare no conflicts of interest.

References

1. Liu, J.Q.; Chen, J.; Zhang, Z.; Ma, J.; Pan, Y.; Ejhieh, N.A.; Lu, C.; Bo, Z. Current status and prospects of MOFs as controlled delivery of Pt anticancer drugs. *Dalton Trans.* **2023**, *52*, 6226–6238.
2. Soliman, S.M.; Fathalla, E.M.; Sharaf, M.M.; El-Faham, A.; Barakat, A.; Haukka, M.; Slawin, A.M.; Woollins, J.D.; Abu-Youssef, M.A. Synthesis, structure and antimicrobial activity of new Co(II) complex with bis-morpholino/benzoimidazole-s-triazine ligand. *Inorganics* **2023**, *11*, 278. [[CrossRef](#)]
3. Gönül, İ.; Burak, A.; Karaca, S.; Şahin, O.; Serin, S. Novel copper(II) complexes of two tridentate ONN type ligands: Synthesis, characterization, electrical conductivity and luminescence properties. *Inorg. Chim. Acta* **2018**, *477*, 75–83. [[CrossRef](#)]
4. Fink, J.K. *The Chemistry of Bio-Based Polymers*; John Wiley & Sons: Hoboken, NJ, USA, 2019.
5. Nedelko, V.V.; Shastin, A.V.; Korsunskii, B.L.; Chukanov, N.V.; Larikova, T.S.; Kazakov, A.I. Synthesis and thermal decomposition of ditetrazol-5-ylamine. *Russ. Chem. Bull.* **2005**, *54*, 1710–1714. [[CrossRef](#)]
6. El-Faham, A.; Dahlous, K.A.; Al Othman, Z.A.; Al-Lohedan, H.A.; El-Mahdy, G.A. sym-Trisubstituted 1,3,5-triazine derivatives as promising organic corrosion inhibitors for steel in acidic solution. *Molecules* **2016**, *21*, 436. [[CrossRef](#)]
7. Mikhaylichenko, S.N.; Patel, S.M.; Dalili, S.; Chesnyuk, A.A.; Zaplishny, V.N. Synthesis and structure of new 1,3,5-triazine-pyrazole derivatives. *Tetrahedron Lett.* **2009**, *50*, 2505–2508. [[CrossRef](#)]
8. Farooq, M.; Sharma, A.; Almarhoon, Z.; Al-Dhfyhan, A.; El-Faham, A.; Taha, N.A.; Wadaan, M.A.; de la Torre, B.G.; Albericio, F. Design and synthesis of mono- and di-pyrazolyl-s-triazine derivatives, their anticancer profile in human cancer cell lines, and in vivo toxicity in zebrafish embryos. *Bioorg. Chem.* **2019**, *87*, 457–464. [[CrossRef](#)] [[PubMed](#)]
9. Mooibroek, T.J.; Gamez, P. The s-triazine ring, a remarkable unit to generate supramolecular interactions. *Inorg. Chim. Acta* **2007**, *360*, 381–404. [[CrossRef](#)]
10. Gamez, P.; Reedijk, J. 1,3,5-Triazine-based synthons in supramolecular chemistry. *Eur. J. Inorg. Chem.* **2006**, *2006*, 29–42. [[CrossRef](#)]
11. Das, A.; Demeshko, S.; Dechert, S.; Meyer, F. A new triazine-based tricompartamental ligand for stepwise assembly of mononuclear, dinuclear, and 1D-polymeric heptacoordinate Manganese(II)/Azido complexes. *Eur. J. Inorg. Chem.* **2011**, *2011*, 1240–1248. [[CrossRef](#)]
12. Golankiewicz, B.; Januszczyk, P.; Ikeda, S.; Balzarini, J.; De Clercq, E. Synthesis and antiviral activity of benzyl-substituted imidazo [1,5-a]-1,3,5-triazine (5,8-diaza-7,9-dideazapurine) derivatives. *J. Med. Chem.* **1995**, *38*, 3558–3565. [[CrossRef](#)] [[PubMed](#)]
13. Lucry, L.; Enoma, F.; Estour, F.; MÉnager, S.; Lafont, O.; Oulyadi, H. Synthesis and biological testing of 3-phenyloctahydro-pyrimido [1,2-a]-s-triazine derivatives. *J. Heterocycl. Chem.* **2002**, *39*, 663–670. [[CrossRef](#)]
14. Chu, J.; Chen, W.; Su, G.; Song, Y.F. Four new copper(II) complexes with di-substituted s-triazine-based ligands. *Inorg. Chim. Acta* **2011**, *376*, 350–357. [[CrossRef](#)]
15. Shanmugakala, R.; Tharmaraj, P.; Sheela, C. Synthesis and spectral studies on metal complexes of s-triazine based ligand and non linear optical properties. *J. Mol. Struct.* **2014**, *1076*, 606–613. [[CrossRef](#)]
16. Katugampala, S.; Perera, I.C.; Nanayakkara, C.; Perera, T. Synthesis, characterization, and antimicrobial activity of novel sulfonated copper-triazine complexes. *Bioinorg. Chem. Appl.* **2018**, *2018*, 2530851. [[CrossRef](#)]
17. Rollas, S.; Güniz Küçükgülzel, Ş. Biological activities of hydrazone derivatives. *Molecules* **2007**, *12*, 1910–1939. [[CrossRef](#)]

18. Jabeen, M. A comprehensive review on analytical applications of hydrazone derivatives. *J. Turk. Chem. Soc. A Chem.* **2022**, *9*, 663–698. [[CrossRef](#)]
19. Kourounakis, A.P.; Xanthopoulos, D.; Tzara, A. Morpholine as a privileged structure: A review on the medicinal chemistry and pharmacological activity of morpholine containing bioactive molecules. *Med. Res. Rev.* **2020**, *40*, 709–752. [[CrossRef](#)]
20. Wang, S.; Li, G.; Huo, Q.; Liu, Y. Syntheses, crystal structures of two coordination polymers constructed from imidazole-based dicarboxylate ligands containing alkyl group. *Inorg. Chem. Commun.* **2013**, *30*, 115–119. [[CrossRef](#)]
21. Zhang, B.J.; Wang, C.J.; Qiu, G.M.; Huang, S.; Zhou, X.L.; Weng, J.; Wang, Y.Y. Polycarboxylate anions effect on the structures of a series of transition metal-based coordination polymers: Syntheses, crystal structures and bioactivities. *Inorg. Chim. Acta* **2013**, *397*, 48–59. [[CrossRef](#)]
22. Kundu, S.; Roy, S.; Bhar, K.; Ghosh, R.; Lin, C.H.; Ribas, J.; Ghosh, B.K. Syntheses, structures and magnetic properties of two one-dimensional coordination polymers of cobalt(II) and nickel(II) dicyanamide containing a tridentate N-donor Schiff base. *J. Mol. Struct.* **2013**, *1038*, 78–85. [[CrossRef](#)]
23. Matsubara, K.; Sueyasu, T.; Esaki, M.; Kumamoto, A.; Nagao, S.; Yamamoto, H.; Koga, Y.; Kawata, S.; Matsumoto, T. Cobalt(II) complexes bearing a bulky N-heterocyclic carbene for catalysis of kumada-tamao-corriu cross-coupling reactions of aryl halides. *Eur. J. Inorg. Chem.* **2012**, *2012*, 3079–3086. [[CrossRef](#)]
24. Matsubara, K.; Kumamoto, A.; Yamamoto, H.; Koga, Y.; Kawata, S. Synthesis and structure of cobalt(II) iodide bearing a bulky N-heterocyclic carbene ligand, and catalytic activation of bromoalkanes. *J. Organomet. Chem.* **2013**, *727*, 44–49. [[CrossRef](#)]
25. Maghami, M.; Farzaneh, F.; Simpson, J.; Ghiasi, M.; Azarkish, M. Synthesis, crystal structure, antibacterial activity and theoretical studies on a novel mononuclear cobalt(II) complex based on 2,4,6-tris(2-pyridyl)-1,3,5-triazine ligand. *J. Mol. Struct.* **2015**, *1093*, 24–32. [[CrossRef](#)]
26. Scarpellini, M.; Neves, A.; Hörner, R.; Bortoluzzi, A.J.; Szpoganics, B.; Zucco, C.; Nome Silva, R.A.; Drago, V.; Mangrich, A.S.; Ortiz, W.A. Phosphate diester hydrolysis and DNA damage promoted by new cis-aqua/hydroxy copper(II) complexes containing tridentate imidazole-rich ligands. *Inorg. Chem.* **2003**, *42*, 8353–8365. [[CrossRef](#)]
27. Singh, V.P.; Katiyar, A.; Singh, S. Synthesis, characterization of some transition metal(II) complexes of acetone p-amino acetophenone salicyloyl hydrazone and their anti microbial activity. *Biometals* **2008**, *21*, 491–501. [[CrossRef](#)]
28. Takeuchi, T.; Böttcher, A.; Quezada, C.M.; Meade, T.J.; Gray, H.B. Inhibition of thermolysin and human α -thrombin by cobalt(III) Schiff base complexes. *Bioorg. Med. Chem.* **1999**, *7*, 815–819. [[CrossRef](#)]
29. Dimiza, F.; Papadopoulos, A.N.; Tangoulis, V.; Psycharis, V.; Raptopoulou, C.P.; Kessissoglou, D.P.; Psomas, G. Biological evaluation of non-steroidal anti-inflammatory drugs-cobalt(II) complexes. *Dalton Trans.* **2010**, *39*, 4517–4528. [[CrossRef](#)]
30. Liang, F.; Wang, P.; Zhou, X.; Li, T.; Li, Z.; Lin, H.; Gao, D.; Zheng, C.; Wu, C. Nickel(II) and cobalt(II) complexes of hydroxyl-substituted triazamacrocyclic ligand as potential antitumor agents. *Bioorg. Med. Chem. Lett.* **2004**, *14*, 1901–1904. [[CrossRef](#)]
31. Maccari, R.; Ottanà, R.; Bottari, B.; Rotondo, E.; Vigorita, M.G. In vitro advanced antimycobacterial screening of cobalt(II) and copper(II) complexes of fluorinated isonicotinoylhydrazones. *Bioorg. Med. Chem. Lett.* **2004**, *14*, 5731–5733. [[CrossRef](#)]
32. Unitt, J.F.; Boden, K.L.; Wallace, A.V.; Ingall, A.H.; Coombs, M.E.; Ince, F. Novel cobalt complex inhibitors of mitochondrial calcium uptake. *Bioorg. Med. Chem.* **1999**, *7*, 1891–1896. [[CrossRef](#)] [[PubMed](#)]
33. McKerrow, J.H.; Sun, E.; Rosenthal, P.J.; Bouvier, J. The proteases and pathogenicity of parasitic protozoa. *Annu. Rev. Microbiol.* **1993**, *47*, 821–853. [[CrossRef](#)] [[PubMed](#)]
34. Ott, I.; Gust, R. Non platinum metal complexes as anti-cancer drugs. *Arch. Pharm. Int. J. Pharm. Med. Chem.* **2007**, *340*, 117–126. [[CrossRef](#)]
35. Huang, P.P.; Wu, T.T.; Tuo, M.Q.; Ge, J.; Huang, P.; Wang, W.Q.; Yang, J.P.; Pan, H.B.; Lu, J.F. Supramolecular complexes of Co(II), Zn(II) and Mn(II) based on a pyridazine dicarboxylic derivative: Synthesis, crystal structures and properties. *J. Mol. Struct.* **2024**, *1307*, 138061. [[CrossRef](#)]
36. Amiri, A.; Mirzaei, M. *Metal–Organic Frameworks in Analytical Chemistry*; The Royal Society of Chemistry: London, UK, 2023. [[CrossRef](#)]
37. Mirzaei, M.; Eshtiagh-Hosseini, M.; Bauzá, A.; Zarghami, S.; Ballester, P.; Maguee, J.T.; Frontera, A. On the importance of non covalent interactions in the structure of coordination Cu(II) and Co(II) complexes of pyrazine- and pyridine-dicarboxylic acid derivatives: Experimental and theoretical views. *CrystEngComm* **2014**, *16*, 6149–6158. [[CrossRef](#)]
38. Mirzaei, M.; Eshtiagh-Hosseini, H.; Karrabi, Z.; Molčanov, K.; Eydizadeh, E.; Maguee, J.T.; Bauzá, A.; Frontera, A. Crystal engineering with coordination compounds of NiII, CoII, and CrIII bearing dipicolinic acid driven by the nature of the noncovalent interactions. *CrystEngComm* **2014**, *16*, 5352–5363. [[CrossRef](#)]
39. Hebrard, F.; Kalck, P. Cobalt-catalyzed hydroformylation of alkenes: Generation and recycling of the carbonyl species, and catalytic cycle. *Chem. Rev.* **2009**, *109*, 4272–4282. [[CrossRef](#)]
40. Junge, K.; Papa, V.; Beller, M. Cobalt–pincer complexes in catalysis. *Chem. Eur. J.* **2019**, *25*, 122–143. [[CrossRef](#)]
41. Pototschnig, G.; Maulide, N.; Schnürch, M. Direct functionalization of C–H bonds by iron, nickel, and cobalt catalysis. *Chem. Eur. J.* **2017**, *23*, 9206–9232. [[CrossRef](#)]
42. Shao, D.; Shi, L.; Wei, H.Y.; Wang, X.Y. Field-induced single-ion magnet behaviour in two new cobalt(II) coordination polymers with 2,4,6-Tris(4-pyridyl)-1,3,5-triazine. *Inorganics* **2017**, *5*, 90. [[CrossRef](#)]
43. Osman, A.H. Synthesis and characterization of cobalt(II) and nickel(II) complexes of some Schiff bases derived from 3-hydrazino-6-methyl[1,2,4] triazin-5(4H)one. *Transit. Met. Chem.* **2006**, *31*, 35–41. [[CrossRef](#)]

44. Menati, S.; Rudbari, H.A.; Askari, B.; Farsani, M.R.; Jalilian, F.; Dini, G. Synthesis and characterization of insoluble cobalt(II), nickel(II), zinc(II) and palladium(II) Schiff base complexes: Heterogeneous catalysts for oxidation of sulfides with hydrogen peroxide. *Comptes Rendus Chim.* **2016**, *19*, 347–356. [[CrossRef](#)]
45. Marandi, F.; Moeini, K.; Arkak, A.; Mardani, Z.; Krautscheid, H. Docking studies to evaluate the biological activities of the Co(II) and Ni(II) complexes containing the triazine unit: Supported by structural, spectral, and theoretical studies. *J. Coord. Chem.* **2018**, *71*, 3893–3911. [[CrossRef](#)]
46. Soliman, S.M.; Elsilk, S.E.; El-Faham, A. Syntheses, structure, Hirshfeld analysis and antimicrobial activity of four new Co(II) complexes with s-triazine-based pincer ligand. *Inorg. Chim. Acta* **2020**, *510*, 119753. [[CrossRef](#)]
47. Soliman, S.M.; Massoud, R.A.; Al-Rasheed, H.H.; El-Faham, A. Syntheses and structural investigations of penta-coordinated Co(II) complexes with bis-pyrazolo-s-triazine pincer ligands, and evaluation of their antimicrobial and antioxidant activities. *Molecules* **2021**, *26*, 3633. [[CrossRef](#)]
48. Fathalla, E.M.; Abu-Youssef, M.A.; Sharaf, M.M.; El-Faham, A.; Barakat, A.; Badr, A.M.; Soliman, S.M.; Slawin, A.M.; Woollins, J.D. Synthesis, characterizations, antitumor and antimicrobial evaluations of novel Mn(II) and Cu(II) complexes with NNN-tridentate s-triazine-schiff base ligand. *Inorg. Chim. Acta* **2023**, *555*, 121586. [[CrossRef](#)]
49. Fathalla, E.M.; Abu-Youssef, M.A.; Sharaf, M.M.; El-Faham, A.; Barakat, A.; Haukka, M.; Soliman, S.M. synthesis, X-ray structure of two hexa-coordinated Ni(II) complexes with s-triazine hydrazine schiff base ligand. *Inorganics* **2023**, *11*, 222. [[CrossRef](#)]
50. Hassan, M.; El-Faham, A.; Barakat, A.; Haukka, M.; Tatikonda, R.; Abu-Youssef, M.A.M.; Soliman, S.M.; Youstri, A. Synthesis, X-ray structure, cytotoxic, and anti-Microbial activities of Zn(II) complexes with a hydrazono s-triazine bearing pyridyl arm. *Inorganics* **2024**, *12*, 176. [[CrossRef](#)]
51. Lever, A.B.P. *Inorganic Electronic Spectroscopy*, 2nd ed.; Elsevier: Amsterdam, The Netherlands, 1984.
52. Addison, A.W.; Rao, T.N.; Reedijk, J.; van Rijn, J.; Verschoor, G.C. Synthesis, structure, and spectroscopic properties of copper(II) compounds containing nitrogen-sulphur donor ligands; the crystal and molecular structure of aqua[1,7-bis(N-methylbenzimidazol-2'-yl)-2,6-dithiaheptane]copper(II) perchlorate. *J. Chem. Soc. Dalton Trans.* **1984**, *7*, 1349–1356. [[CrossRef](#)]
53. Lu, J.F.; Huang, P.; Zhang, D.; Wang, Q.; Zheng, N.; Wu, R.; Liu, Q.; Jin, L.X.; Yu, X.H.; Ji, X.H.; et al. 1-(3-Amino-4-morpholino-1H-indazole-1-carbonyl)-N-phenylcyclopropane-1-carboxamide: Design, synthesis, crystal structure, antitumor activity, DFT and Hirshfeld surface analysis. *J. Mol. Struct.* **2020**, *1210*, 127996. [[CrossRef](#)]
54. Huang, P.; Zhao, J.; Gao, Y.H.; Jin, L.X.; Wang, Q.; Yu, X.H.; Lu, J.F. N-{2-[(2-chlorothieno[3,2-d]pyrimidin-4-yl)amino]ethyl}-3-methoxybenzamide: Design, synthesis, crystal structure, antiproliferative activity, DFT, Hirshfeld surface analysis and molecular docking study. *J. Biomol. Struct. Dyn.* **2020**, *40*, 787–795. [[CrossRef](#)] [[PubMed](#)]
55. Zhang, Y.; Su, Y.X.; Cai, Z.; Tong, L.; Dong, W.K. Structural, fluorescent and theoretical studies of a more flexible salamo-type ligand and its uncommon tetranuclear chloride-bridged nickel(II) complex. *J. Mol. Struct.* **2024**, *1309*, 138164. [[CrossRef](#)]
56. Gan, L.L.; Niu, H.Y.; Liu, L.L.; Dong, W.K.; Ding, Y.J. The effect of different counter-anions on two nonsymmetric salamo-type copper(II) complexes with different structures. *J. Mol. Struct.* **2024**, *1302*, 137526. [[CrossRef](#)]
57. Ding, Y.F.; Man, L.L.; Tong, L.; Li, X.; Dong, W.K.; Ding, Y.J. Differently structural Cu(II) and Ni(II) complexes of a nonsymmetrical tetradentate half-salamo like N3O-donor ligand: Synthesis, crystal structure, spectral properties and theoretical studies. *J. Mol. Struct.* **2024**, *1301*, 137341. [[CrossRef](#)]
58. Tong, L.; Ding, Y.F.; Li, X.; Man, L.L.; Dong, W.K. Synthesis, crystal structure, fluorescence properties, and theoretical studies of a dinuclear Ni(II) complex derived from a quinoline-containing half-salamo-type ligand. *J. Coord. Chem.* **2023**, *76*, 1635–1649. [[CrossRef](#)]
59. Tabti, S.; Aggoun, D.; Aref, D.; Sawafta, A.; Djedouani, A.; Abu-Rayyan, A.; AlObaid, A.; Lhoste, J.; Robert, C.; Augste, S.; et al. Spectral, crystal structure of novel Pyran-2-one Zwitterion Schiff derivative: Thermal, Physicochemical, DFT/HSA-interactions, enol↔imine tautomerization and anticancer activity. *J. Mol. Struct.* **2024**, *1310*, 138258. [[CrossRef](#)]
60. Aouad, M.R.; Messali, M.; Rezki, N.; Al-Zaqri, N.; Warad, I. Single proton intramigration in novel 4-phenyl-3-((4-phenyl-1H-1,2,3-triazol-1-yl)methyl)-1H-1,2,4-triazole-5(4H)-thione: XRD-crystal interactions, physicochemical, thermal, Hirshfeld surface, DFT realization of thiol/thione tautomerism. *J. Mol. Liq.* **2018**, *264*, 621–630. [[CrossRef](#)]
61. Abu Saleemh, F.; Musameh, S.; Sawafta, A.; Brandao, P.; Tavares, C.J.; Ferdov, S.; Barakat, A.; Al Ali, A.; Al-Noaimi, M.; Warad, I. Diethylenetriamine/diamines/copper(II) complexes [Cu(dien)(NN)]Br₂: Synthesis, solvatochromism, thermal, electrochemistry, single crystal, Hirshfeld surface analysis and antibacterial activity. *Arab. J. Chem.* **2017**, *10*, 845–854. [[CrossRef](#)]
62. Christian, J.; Ejsmont, K.; Huder, L. The enrichment ratio of atomic contacts in crystals, an indicator derived from the Hirshfeld surface analysis. *IUCr* **2014**, *1*, 119–128.
63. Turner, M.J.; Thomas, S.P.; Shi, M.W.; Jayatilaka, D.; Spackman, M.A. Energy frameworks: Insights into interaction anisotropy and the mechanical properties of molecular crystals. *Chem. Commun.* **2015**, *51*, 3735–3738. [[CrossRef](#)]
64. Bakheit, A.H.; Attwa, M.W.; Kadi, A.A.; Alkahtani, H.M. Structural Analysis and Reactivity Insights of (E)-Bromo-4-((4-((1-(4-chlorophenyl) ethylidene) amino)-5-phenyl-4H-1,2,4-triazol-3-yl) thio)-5-((2-isopropylcyclohexyl) oxy) Furan-2(5H)-one: A combined approach using single-crystal X-ray diffraction, Hirshfeld surface analysis, and conceptual density functional theory. *Crystals* **2023**, *13*, 1313. [[CrossRef](#)]
65. Turner, M.J.; Grabowsky, S.; Jayatilaka, D.; Spackman, M.A. Accurate and efficient model energies for exploring intermolecular interactions in molecular crystals. *J. Phys. Chem. Lett.* **2014**, *5*, 4249–4255. [[CrossRef](#)] [[PubMed](#)]

66. Hajji, M.; Mtiraoui, H.; Amiri, N.; Msaddek, M.; Guerfel, T. Crystallographic and first-principles density functional theory study on the structure, noncovalent interactions, and chemical reactivity of 1,5-benzodiazepin-2-ones derivatives. *Int. J. Quantum Chem.* **2019**, *119*, e26000. [[CrossRef](#)]
67. Abad, N.; Sallam, H.H.; Al-Ostoot, F.H.; Khamees, H.A.; Al-horaibi, S.A.; Khanum, S.A.; Madegowda, M.; El Hafi, M.; Mague, J.T.; Essassi, E.M. Synthesis, crystal structure, DFT calculations, Hirshfeld surface analysis, energy frameworks, molecular dynamics and docking studies of novel isoxazolequinoxaline derivative (IZQ) as anti-cancer drug. *J. Mol. Struct.* **2021**, *1232*, 130004. [[CrossRef](#)]
68. Edwards, A.J.; Mackenzie, C.F.; Spackman, P.R.; Jayatilaka, D.; Spackman, M.A. Intermolecular interactions in molecular crystals: What's in a name? *Farad. Disc.* **2017**, *203*, 93–112. [[CrossRef](#)] [[PubMed](#)]
69. Mackenzie, C.F.; Spackman, P.R.; Jayatilaka, D.; Spackman, M.A. CrystalExplorer model energies and energy frameworks: Extension to metal coordination compounds, organic salts, solvates and open-shell systems. *IUCr* **2017**, *4*, 575–587. [[CrossRef](#)] [[PubMed](#)]
70. Wang, K.; He, X.; Rong, C.; Zhong, A.; Liu, S.; Zhao, D. On the origin and nature of internal methyl rotation barriers: An information-theoretic approach study. *Theor. Chem. Acc.* **2022**, *141*, 68. [[CrossRef](#)]
71. Zhong, A.; Chen, D.; Li, R. Revisiting the beryllium bonding interactions from energetic and wavefunction perspectives. *Chem. Phys. Lett.* **2015**, *633*, 265–272. [[CrossRef](#)]
72. Tan, S.L.; Jotani, M.M.; Tiekink, E.R. Utilizing Hirshfeld surface calculations, non-covalent interaction (NCI) plots and the calculation of interaction energies in the analysis of molecular packing. *Acta Cryst.* **2019**, *E75*, 308–318. [[CrossRef](#)]
73. Sreenatha, N.; Chakravarthy, A.J.; Suchithra, B.; Lakshminarayana, B.; Hariprasad, S.; Ganesh, D. Crystal, spectral characterization, molecular docking, Hirshfeld computational studies and 3D-energy framework analysis of a novel puckered compound (C₁₄H₁₅ClO): 2-Chloro-3-phenyl-5,5-dimethylcyclohex-2-en-1-one. *J. Mol. Struct.* **2020**, *1210*, 127979. [[CrossRef](#)]
74. Guo, Z.A.; Xian, J.Y.; Rong, L.R.; Qin, H.; Jie, Z. Theoretical study of metal ion impact on geometric and electronic properties of terbutaline compounds. *Monatsh. Chem.* **2019**, *150*, 1355–1364. [[CrossRef](#)]
75. Refaat, H.M.; Alotaibi, A.A.M.; Dege, N.; El-Faham, A.; Soliman, S.M. Co(II) complexes based on the bis-pyrazol-s-triazine pincer ligand: Synthesis, X-ray structure studies, and cytotoxic evaluation. *Crystals* **2022**, *12*, 741. [[CrossRef](#)]
76. Rikagu Oxford Diffraction. *CrysAlisPro*; Rikagu Oxford Diffraction Inc.: Oxfordshire, UK, 2020.
77. Sheldrick, G.M. SHELXT—Integrated space-group and crystal-structure determination. *Acta Cryst.* **2015**, *71*, 3–8. [[CrossRef](#)] [[PubMed](#)]
78. Sheldrick, G.M. Crystal structure refinement with SHELXL. *Acta Cryst.* **2015**, *C71*, 3–8.
79. Hübschle, C.B.; Sheldrick, G.M.; Dittrich, B. ShelXle: A Qt graphical user interface for SHELXL. *J. Appl. Cryst.* **2011**, *44*, 1281–1284. [[CrossRef](#)]
80. Spackman, M.A.; Jayatilaka, D. Hirshfeld surface analysis. *CrystEngComm* **2009**, *11*, 19–32. [[CrossRef](#)]
81. Turner, M.; McKinnon, J.; Wolff, S.; Grimwood, D.; Spackman, P.; Jayatilaka, D.; Spackman, M. *CrystalExplorer17*; University of Western Australia: Perth, Australia, 2017.
82. Chai, J.D.; Head-Gordon, M. Long-range corrected hybrid density functionals with damped atom–atom dispersion corrections. *Phys. Chem.* **2008**, *10*, 6615–6620. [[CrossRef](#)]
83. Frisch, M.; Clemente, F.; Frisch, M.J.; Trucks, G.W.; Schlegel, H.B.; Scuseria, G.E.; Robb, M.A.; Cheeseman, J.R.; Scalmani, G.; Barone, V.; et al. Uranyl extraction by N,N-dialkylamide ligands studied by static and dynamic DFT simulations. In *Gaussian 09*; Gaussian Inc.: Wallingford, UK, 2009.
84. Dennington, R.D., II; Keith, T.; Millam, J. *GaussView*, Version 4.1; Semicem Inc.: Shawnee Mission, KS, USA, 2007.
85. Mosmann, T. Rapid colorimetric assay for cellular growth and survival: Application to proliferation and cytotoxicity assays. *J. Immunol. Methods* **1983**, *65*, 55–63. [[CrossRef](#)]
86. Lu, P.L.; Liu, Y.C.; Toh, H.S.; Lee, Y.L.; Liu, Y.M.; Ho, C.M.; Huang, C.C.; Liu, C.E.; Ko, W.C.; Wang, J.H. Epidemiology and antimicrobial susceptibility profiles of Gram-negative bacteria causing urinary tract infections in the Asia-Pacific region: 2009–2010 results from the Study for Monitoring Antimicrobial Resistance Trends (SMART). *Int. J. Antimicrob. Agents* **2012**, *40*, S37–S43. [[CrossRef](#)]

Disclaimer/Publisher's Note: The statements, opinions and data contained in all publications are solely those of the individual author(s) and contributor(s) and not of MDPI and/or the editor(s). MDPI and/or the editor(s) disclaim responsibility for any injury to people or property resulting from any ideas, methods, instructions or products referred to in the content.